Supporting Information

# Computational screening of efficient graphene-supported transition metal single atom catalysts toward oxygen reduction reaction

Lei Li, Rao Huang, Xinrui Cao and Yuhua Wen*

Department of Physics, Xiamen University, Xiamen 361005, China.

E-mail: yhwen@xmu.edu.cn

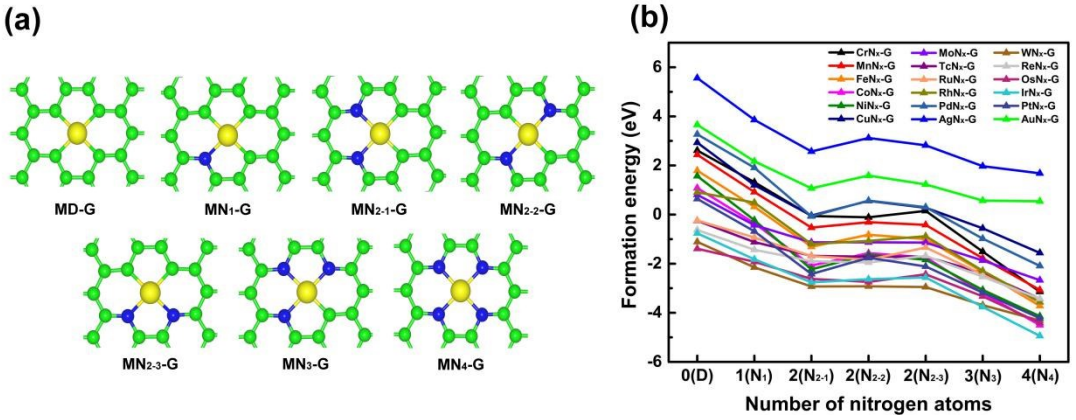


**Fig. S1.** (a) Schematic structures and (b) formation energy of $MN_x$-G. The green, blue, and yellow spheres denote C, N, and M atoms, respectively.

**Table S1.** The binding energy ($E_b$) of $MN_4$-G and cohesive energy ($E_c$) of bulk M.

| M | $E_b$ (eV) | $E_c$ (eV) | M | $E_b$ (eV) | $E_c$ (eV) | M | $E_b$ (eV) | $E_c$ (eV) |
|---|---|---|---|---|---|---|---|---|
| Cr | 6.91 | 4.14 | Mo | 6.45 | 6.36 | W | 8.08 | 8.48 |
| Mn | 6.84 | 3.87 | Tc | 7.20 | 7.09 | Re | 7.20 | 7.81 |
| Fe | 7.49 | 4.94 | Ru | 7.35 | 6.88 | Os | 8.18 | 8.32 |

| | | | | | | | | |
|---|---|---|---|---|---|---|---|---|
| Co | 7.84 | 5.13 | Rh | 7.33 | 5.63 | Ir | 8.71 | 7.23 |
| Ni | 7.91 | 4.88 | Pd | 5.86 | 3.70 | Pt | 7.99 | 5.47 |
| Cu | 5.33 | 3.48 | Ag | 2.09 | 2.49 | Au | 3.20 | 2.98 |

**Table S2.** The adsorption height of M atom ($d_1$), average M–N bond length ($d_2$), and Bader charges analysis ($\Delta$q) for $MN_4$-G. Note that the minus sign in $\Delta$q denotes electron loss.

| M | $d_1$ (Å) | $d_2$ (Å) | Δq (e) | | | M | $d_1$ (Å) | $d_2$(Å) | Δq (e) | | |
|---|---|---|---|---|---|---|---|---|---|---|---|
| | | | $N_4$ | M | G | | | | $N_4$ | M | G |
| Cr | 0.134 | 1.941 | 0.52 | -1.25 | 0.73 | Tc | 0.493 | 1.989 | 0.26 | -1.23 | 0.97 |
| Mn | 0.002 | 1.910 | 0.21 | -1.28 | 1.07 | Ru | 0.469 | 1.968 | 0.17 | -0.91 | 0.74 |
| Fe | 0.012 | 1.894 | 0.09 | -1.09 | 1.00 | Rh | 0.062 | 1.944 | 0.26 | -0.66 | 0.40 |
| Co | 0.010 | 1.878 | 0.06 | -0.88 | 0.82 | Pd | 0.015 | 1.952 | 0.28 | -0.71 | 0.43 |
| Ni | 0.009 | 1.883 | 0.02 | -0.84 | 0.82 | Ir | 0.053 | 1.941 | 0.28 | -0.76 | 0.48 |
| Cu | 0.008 | 1.923 | 0.38 | -0.92 | 0.54 | Pt | 0.033 | 1.953 | 0.29 | -0.75 | 0.46 |
| Mo | 0.825 | 2.045 | 0.25 | -1.26 | 1.01 | Au | 0.033 | 1.967 | 0.15 | -0.96 | 0.81 |

**Table S3.** Relative Energy of $O_2$ adsorbed on $MN_4$-G. Note that the energy of the most stable configuration is defined as 0.000 eV and '--' indicates these configurations are not stable.

| M | Δ*E* (eV) | | | | |
|---|---|---|---|---|---|
| | Side-A | Side-B | Side-C | End-A | End-B |
| Cr | 0.000 | -- | -- | 0.533 | 0.460 |
| Mn | 0.000 | -- | -- | 0.510 | 0.418 |
| Mo | -- | 0.000 | 0.068 | -- | -- |
| Tc | -- | 0.000 | 0.160 | 0.713 | -- |
| Fe | 0.394 | -- | -- | 0.196 | 0.000 |
| Co | -- | -- | -- | 0.088 | 0.000 |
| Ru | -- | 0.118 | -- | -- | 0.000 |
| Rh | 0.845 | -- | -- | 0.086 | 0.000 |
| Ir | 0.697 | -- | -- | 0.339 | 0.000 |

**Table S4.** Relative energy of $O_2$ dissociated product.

| M | Δ*E* (eV) | | | | | M | Δ*E* (eV) | | | | |
|---|---|---|---|---|---|---|---|---|---|---|---|
| | $T_1T_1$-A | $T_1T_1$-B | $T_1T_2$ | $T_1B_1$ | $T_1B_2$ | | $T_1T_1$-A | $T_1T_1$-B | $T_1T_2$ | $T_1B_1$ | $T_1B_2$ |
| Fe | -- | -- | 0.298 | 0.000 | 0.048 | Cr | 0.315 | 0.000 | 0.770 | 0.976 | 1.048 |
| Co | -- | 0.494 | 0.126 | 0.000 | 0.097 | Mn | 0.127 | 0.000 | 0.327 | 0.042 | 0.179 |
| Ru | 0.011 | 0.000 | 0.402 | 0.168 | 0.430 | Mo | 0.325 | 0.000 | -- | 1.944 | 2.362 |
| Rh | 1.002 | 1.082 | 0.305 | 0.000 | 0.195 | Tc | 0.209 | 0.000 | 1.208 | 0.992 | 1.376 |
| Ir | 0.096 | 0.325 | 0.269 | 0.000 | 0.281 | | | | | | |

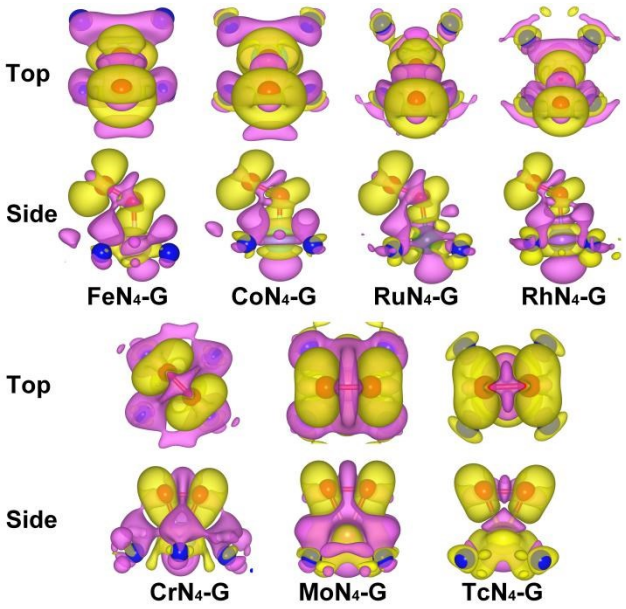


**Fig. S2.** Distribution of exchange charges between $O_2$ and $MN_4$-G with the isovalue of 0.006 eÅ$^{-3}$. Purple and yellow bubbles represent positive and negative charges, respectively.

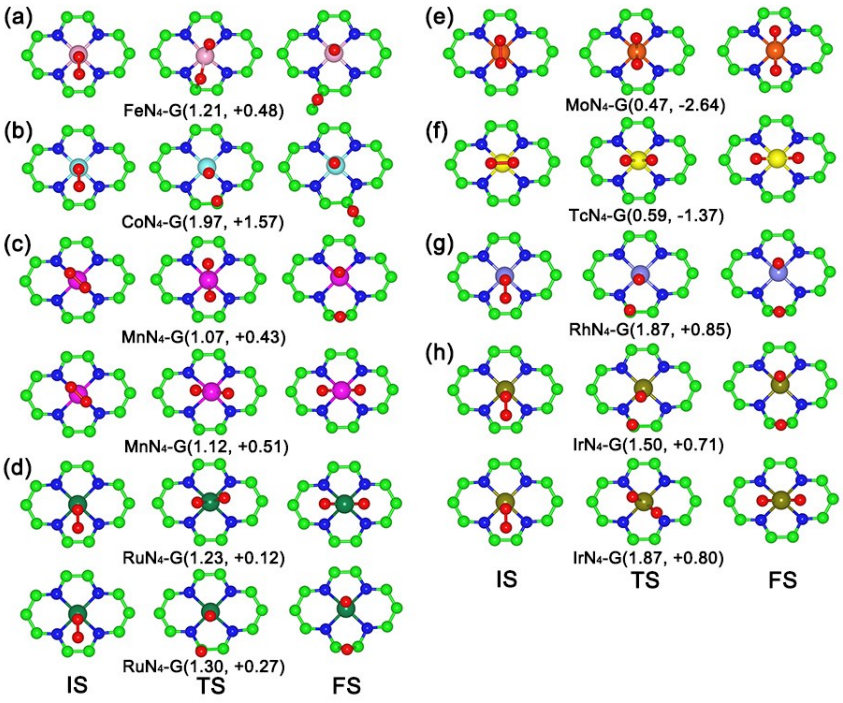


**Fig. S3.** Atomic structures of IS, TS, and FS for the possible path of $O_2$ dissociation on $MN_4$-G supports. The numbers in parenthesis are the energy barriers (left) and reaction energies (right) in units of eV.